Intradermally Focused Infrared Laser Pulses: Thermal Effects at Defined Tissue Depths

Misbah Huzaira Khan, MD,[1]* R. Kehl Sink, PhD,[2] Dieter Manstein, MD,[1] David Eimerl, PhD,[3] and R. Rox Anderson, MD[1]

[1]*Wellman Laboratories of Photomedicine, Department of Dermatology, Harvard Medical School, Boston, Massachusetts 02114*

[2]*Reliant Technologies, Inc., Palo Alto, California*

[3]*EIMEX Software and Consulting, Livermore, California*

Background and Objectives: To produce controlled, spatially confined thermal effects in dermis.

Study Designs/Materials and Methods: A 1 W, 1,500 nm fiber-coupled diode laser was focused with a high numerical aperture (NA) objective to achieve a tight optical focus within the upper dermis of skin held in contact with a glass window. The delivery optics was moved using a computer-controlled translator to generate an array of individual exposure spots. Fresh human facial skin samples were exposed to a range of pulse energies at specific focal depths, and to a range of focal depths at constant pulse energy. Cellular damage was evaluated in frozen sections using nitro-blue tetrazolium chloride (NBTC), a lactate dehydrogenase (LDH) activity stain. Loss of birefringence due to thermal denaturation of collagen was evaluated using cross-polarized light microscopy. The extent of focal thermal injury was compared with a model for photon migration (Monte Carlo Simulation), heat diffusion, and protein denaturation (Arrhenius model).

Results: Arrays of confined, microscopic intradermal foci of thermal injury were created. At high NA, epidermal damage was avoided without active cooling. Foci of thermal injury were typically 50–150 μm in diameter, elliptical, and at controllable depths from 0 to 550 μm. Both LDH inactivation and extracellular matrix denaturation were achieved.

Conclusion: Spatially confined foci of thermal effects can be achieved by focusing a low-power infrared laser into skin. Size, depth, and density of microscopic, thermal damage foci may be arbitrarily controlled while sparing surrounding tissue. This may offer a new approach for nonablative laser therapy of dermal disorders.

Key words: intradermal focusing; focused laser pulses; near infrared laser; photorejuvenation

INTRODUCTION

A variety of highly effective, ablative methods have been used to treat facial rhytides associated with photoaging. These include laser resurfacing, dermabrasion, and chemical peels. These methods completely disrupt or remove the epidermis. Subsequent loss of barrier function results in discomfort and desiccation-induced extension of the original wound depth [1]. Transudation, focal crusting, and edema are generally observed during the period of dermal exposure [2–4]. Epidermal loss also increases the risk of infection, scarring, and pigmentary changes. Stimulation of new extracellular matrix deposition appears to be the primary mechanism for wrinkle reduction [4–6]. Since the microscopic changes associated with wrinkles occur primarily in the dermis, epidermal damage may be unnecessary for treatment of facial rhytides [7–9].

Nonablative dermal remodeling (NDR), also called nonablative skin rejuvenation or subsurfacing, which does not remove the epidermis, was specifically developed as a better-tolerated alternative to ablative laser resurfacing. NDR uses mid-infrared lasers (at wavelengths absorbed by water) in combination with cooling at the skin surface to produce an "upside-down" thermal burn. A 1.32-μm Nd:YAG laser and a 1.45-μm semiconductor diode laser are in clinical use, in combination with dynamic cryogen spray cooling [10]. NDR may also affect dermal targets such as sebaceous follicles; the latter device has recently been approved as a treatment for acne vulgaris [11]. The main problem with NDR, however, is poor and/or unpredictable efficacy compared with ablative treatments. Even when dosimetry is pushed to the point of significant pain and occasional scarring, the efficacy of NDR for treatment of photoaging is limited [12,13].

Selective photothermolysis (SP) is a widely used approach to laser treatment, in which microscopic target structures such as blood vessels, pigmented cells, or hair follicles are preferentially photocoagulated by selectively absorbed pulses of light [14]. Unlike NDR, SP is generally effective and very well tolerated. Some improvement of facial wrinkles occurs after treatment of telangiectases by SP with a pulsed dye laser [15]; this improvement might be stimulated by microscopic thermal damage to the perivascular dermis. We surmised that producing many microscopic regions of thermal injury surrounded by uninjured dermal tissue might achieve a better combination of

*Correspondence to: Misbah Huzaira Khan, MD, Beckman Laser Institute and Medical Clinic, 1002 Health Sciences Road East, University of California, Irvine, Irvine, CA. 92612.
E-mail: mhkhan@uci.edu

Accepted 21 December 2004
Published online in Wiley InterScience (www.interscience.wiley.com).
DOI 10.1002/lsm.20142

efficacy and safety for treatment of photoaging than other treatment modalities. Unlike SP, which depends on specific light-absorbing target structures, arbitrary patterns of microscopic photothermal injury might be created in skin, for example, in arrays, by controlling a tightly focused laser beam. The ability to focus near-infrared lasers well into the dermis has been demonstrated, for example, as the basis for in vivo confocal laser scanning microscopy [16].

It has also been demonstrated that confined dermal damage with epidermal sparing can be obtained with an intradermally focused infrared fiber laser ($\lambda = 1.06$ and 1.2 μm) when exposure times of about 1 second were performed in parallel with surface cooling [17].

Very high power densities can be achieved at an intradermal focus, even with low power lasers.

This study reports confined dermal areas of thermal damage created with a low-power (1 W) infrared diode laser source without surface cooling. This was accomplished through the proper choice of wavelength and numerical aperture (NA) of the focusing lens. The experimental system included focusing optics and a translation stage; exposure durations were in the range of 3–20 milliseconds, which represented only 1% of the laser duty cycle. The analysis of the histological samples revealed that this system could achieve foci of thermal injury within the skin with controllable size, depth, and packing density of the foci. It was possible to either include or avoid epidermal injury without active cooling by proper choice of exposure parameters and delivery optics. The thermal damage pattern as obtained by histology was in good correlation with the damage pattern as predicted by modeling. These results suggest that studies to investigate the clinical effects of various thermal damage patterns may be worthwhile.

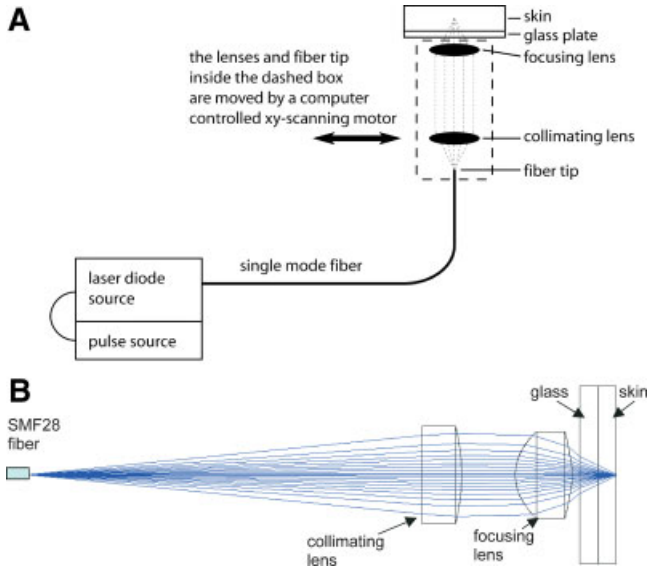

Fig. 1. **A**: Schematic showing laser exposure system; **(B)** ray tracing model showing the optical path from the fiber tip to the beam focus within the skin. [Figure can be viewed in color online via www.interscience.wiley.com.]

METHODS

Optical System

The optical system consisted of a laser source, focusing optics, a window held against the skin, and a translation stage (Reliant FSR investigational device, Reliant Technologies, Inc., Palo Alto, CA). The outputs of four semiconductor laser diodes were combined using polarization and wavelength beam combination. The wavelengths of the lasers were 1,492 and 1,508 nm, with approximately equal power at each wavelength. Combined output of the laser diodes was coupled into a single-mode fused silica fiber. Output from the single mode fiber was collimated and then focused into the skin as shown schematically in Figure 1A, through a 0.9-mm thick glass plate (fused silica, $n = 1.44$). The lenses and one side of the glass plate were antireflection coated to maximize the power coupled into the skin. Focal spot diameter was estimated using a standard knife edge measurement to be less than 20 μm [18]. The effective NA of the focused beam used for this experiment is 0.66. A ray tracing description of the optical design is shown in Figure 1B. The depth of the focal spot within skin samples held against the glass plate was adjusted by varying the spacing between the focusing optics and the glass plate. The lenses and fiber tip were translated by a computer-driven XY-scanning stage to create an array of sequential exposures, with a center-to-center spacing between adjacent spots of 500 μm. Laser exposures and motion of the scanning stage were controlled by software that sequentially stopped the XY-scanning stage at each grid point, turned on the lasers to produce a square-wave pulse of specified pulse duration, and then moved to the next grid point. The pulse duration was controlled with a waveform generator (model 33120A, Agilent Technologies, Inc., Palo Alto, CA).

Ex Vivo Skin Exposures

The study was performed on freshly excised human facial skin upon approval form the Institutional Review Board of Harvard Medical School. Freshly excised, full-thickness human facial skin samples were obtained from the dermatologic surgery clinic at the Massachusetts General Hospital, Boston, MA (from Victor A. Neel, MD, PhD) and trimmed to a 4×6 mm rectangle with a thin layer of subcutaneous fat on the lower surface. A thin layer of aqueous fructose solution designed to match refractive index of skin (Laser Lotion, Palomar Medical Products, Burlington, MA) was applied between the skin sample and glass plate. The entire device was equilibrated at room temperature and no active cooling was provided to the handpiece aperture. Skin samples equilibrated at room temperature ($\sim 25^{\circ}$C) were gently compressed against the glass plate and irradiated.

Laser Exposure Parameters

Samples were divided into two groups. In Group 1, the optical beam was focused at various depths while keeping laser pulse energy constant. In Group 2, the optical beam

TABLE 1. Optical Pulse Parameters Used for Comparing the Effects of Pulse Energy and Focus Depth on Damage Profile for Spatially Confined Thermal Lesions Within the Skin

Sample group	Pulse duration (millisecond)	Power (mW)	Focal depth (μm)
Group 1	12	1,000	50
	12	1,000	200
	12	1,000	450
	12	1,000	600
Group 2	3	1,000	50
	4	1,000	200
	12	1,000	450
	20	1,000	600

was focused to the same depths as in Group 1. Laser pulse energy in Group 2 was adjusted to approximately compensate for optical attenuation at the particular focal depth (see Table 1).

Tissue Microscopy

Fresh frozen, vertical serial sections of the skin samples after laser exposure were prepared for light microscopic analysis. Average frozen section thickness was approximately 10 μm. The sections were stained at room temperature with nitro-blue tetrazolium chloride (NBTC). Reduction of NBTC by lactate dehydrogenase (LDH) leads to an intense blue precipitate. LDH is a thermolabile enzyme; loss of LDH activity subsides rapidly upon heat induced cell damage and is correlated with cell lethality [19,20]. Loss of NBTC staining as described below was used to measure spatial depth and lateral extent of cellular photothermal damage. Dermal collagen denaturation was determined by cross-polarized light microscopy and identified by the loss of dermal collagen birefringence of the same skin sections [21]. The spatial extent of birefringence loss was blindly measured as described below. Loss of birefringence is due to thermal denaturation (melting) of type I collagen, which occurs at a higher temperature than loss of LDH activity. In this study, these endpoints reflect photothermal injury to extracellular matrix and cells, respectively. Routine H&E staining of frozen sections was also performed for light microscopy.

Statistical Analysis

Approximately one hundred laser exposure spots created by each laser parameter in both groups were blindly measured using a calibrated microscope. Loss of NBTC staining (LDH activity) was the most sensitive endpoint indicating the presence of a laser exposure spot. Magnified images (6×) of the thermal lesions were captured with a CCD camera and analyzed blindly using a Visual Basic program. Images of a calibration scale were also captured, to quantify length. Spatial extent of each tissue lesion was measured by selecting 5–10 points around the apparent margin of the lesion, which were then connected to form a polygon. Each point was referenced to the top of the epidermis, which was considered to be at zero depth. The total area of the polygon was estimated by summing the segmental areas for each 10-μm depth interval. These segmental areas were divided by the 10-μm depth interval to yield the estimated diameter of the lesion at each of the depth intervals. The top, maximum depth, maximum diameter of the lesion, and the depth of maximum diameter were also measured using the same program. Typical lesion shapes for various laser exposures and depths were reconstructed from these data based on the measured lesion diameters at each depth segment. Contour plots, as shown in Figure 2C, illustrate the results of this process. The inner contour in each figure shows the diameter at each depth for which 80% of the lesions measured for that particular exposure condition had diameters that were less than or equal to the contour diameter at that particular depth. The outer contour in each figure is drawn at diameters for which 90% of the lesions measured had diameters less than or equal to the contour diameter at that particular depth. Because the data are taken from vertical sections that are not necessarily along the center axis of the lesion, the median radius at each depth (50% contour) is somewhat less than the actual lesion diameter, due to spatial sampling. Because the 80% or 90% contours are considered to be more representative of the actual extent of thermal lesions for each set of conditions sampled, the 50% contours are not shown in the figures.

Optical and Thermal Plots

Modeling of the lesions was carried out using an ab initio formulation of the laser-tissue interaction. Propagation of light through the tissue was calculated using a standard Monte Carlo approach [21] to scattering and absorption. Monte Carlo calculations were first performed using the Henyey-Greenstein [22] scattering profile. To test the sensitivity of the results to the specific choice of scattering profile, calculations were also performed using two other scattering profiles. The second profile used was a simple Gaussian profile, which is more sharply peaked into forward scattering than the standard Henyey-Greenstein model. The third profile was specifically calculated to reflect the properties of scattering from collagen fibers. Collagen is known to self-assemble into structures with a regular geometric cross-section, such as a triangle or hexagon. The scattering for several of these structures was calculated using a segmented laser beam approximation that accounts for both refraction and diffraction without requiring a full electromagnetic wave simulation such as that used in Mie scattering. The scattering profile is relatively insensitive to the assumed shape of the fibers, but depends strongly on the index difference between the fibers and the surrounding medium. At high scattering angles, scattering in this model is considerably stronger than a Henyey-Greenstein model. Thus the second and third profiles have, respectively, significantly lower and higher wide-angle scattering than the standard Henyey-Greenstein model. In general, photon migration was not significantly different for the three scattering profiles, suggesting that the details of the profile are less important than the gross features such as

the angular half-width scattering (θ_{scatt}) and the scattering coefficient (μ_s). Some adjustment of the material constants was allowed in modeling the lesions. In our modeling we tested the sensitivity to variations of the scattering coefficient (μ_s) in the range 60–100/cm and the angular half-width of the scattering (θ_{scatt}) in the range 5–15 degrees. It was found that the model was relatively insensitive to changes over these two ranges. As the parameters varied over this range, the general location and shape of the calculated lesions varied gently and were similar. The depth and width of the different zones of the lesion varied by about 20% and 5%, respectively, a level which is comparable to the variation in the experimental data. The values used to create the plots shown in Figures 2–7 were $\mu =$ 60/cm, and $\theta_{scatt} = 5$ degrees.

The skin is modeled as a series of uniform planar layers, where each layer is characterized by its absorption, thermal conductivity, and specific heat. For the wavelength range of interest, the absorption coefficient in skin is determined by multiplying the water content of the skin by the absorption coefficient in water [23]. The absorption of the tissue (α) was obtained assuming a water fraction of 70% in the tissue, and lies in the range $10 < \alpha < 20$/cm. The theoretical calculations presented in Figures 2–7 were produced using $\alpha = 13$/cm. Heat transport was treated using a standard model of diffusion [21]. The diffusion model was implemented using alternating direction implicit mathematical methods [24] and with adiabatic boundary conditions. While the model is fully three-dimensional, cylindrical symmetry was assumed. The thermal conductivity of the

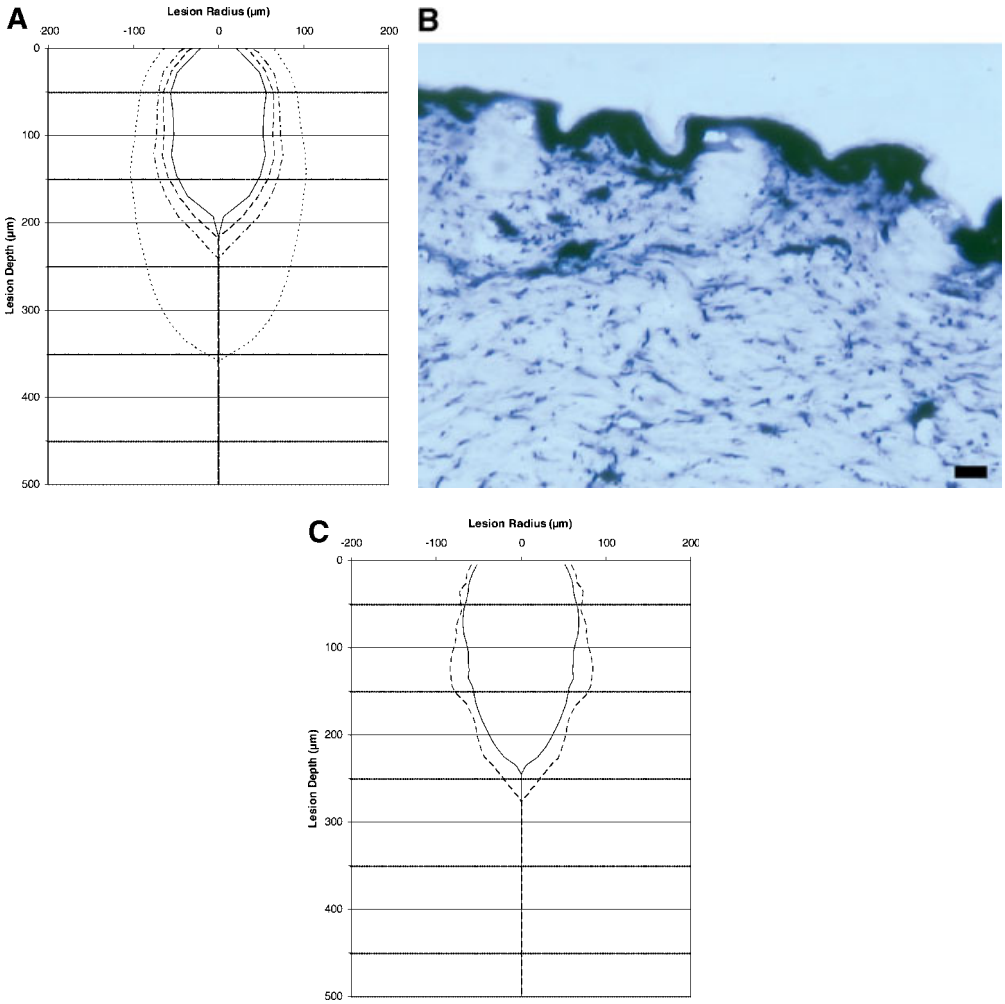

Fig. 2. Exposure parameters: 12 and 3 mJ, respectively, at a focal depth of 50 μm. **A**: Computer simulations of these treatment parameters. Contours are drawn for reaction coordinates of the Arrhenius model ($x = 10^{-2}$, 10^0, 10^2, and 10^4). Note: Only $x = 10^4$ is visible for Figure 3A because the other contours have a radius of approximately 0 for all depths. **B**: NBTC-stained histologic sections of ex vivo facial skin, immediately after exposure (6×, scale bar, 50 μm). **C**: Statistical contours representing the extent of thermal damage. Note that depth of thermal damage is reduced substantially with reduced pulse energy. (Contours are drawn at diameters for which 80% and 90% of the lesions measured had diameters less than or equal to the contour diameter at that particular depth.) [Figure can be viewed in color online via www.interscience.wiley.com.]

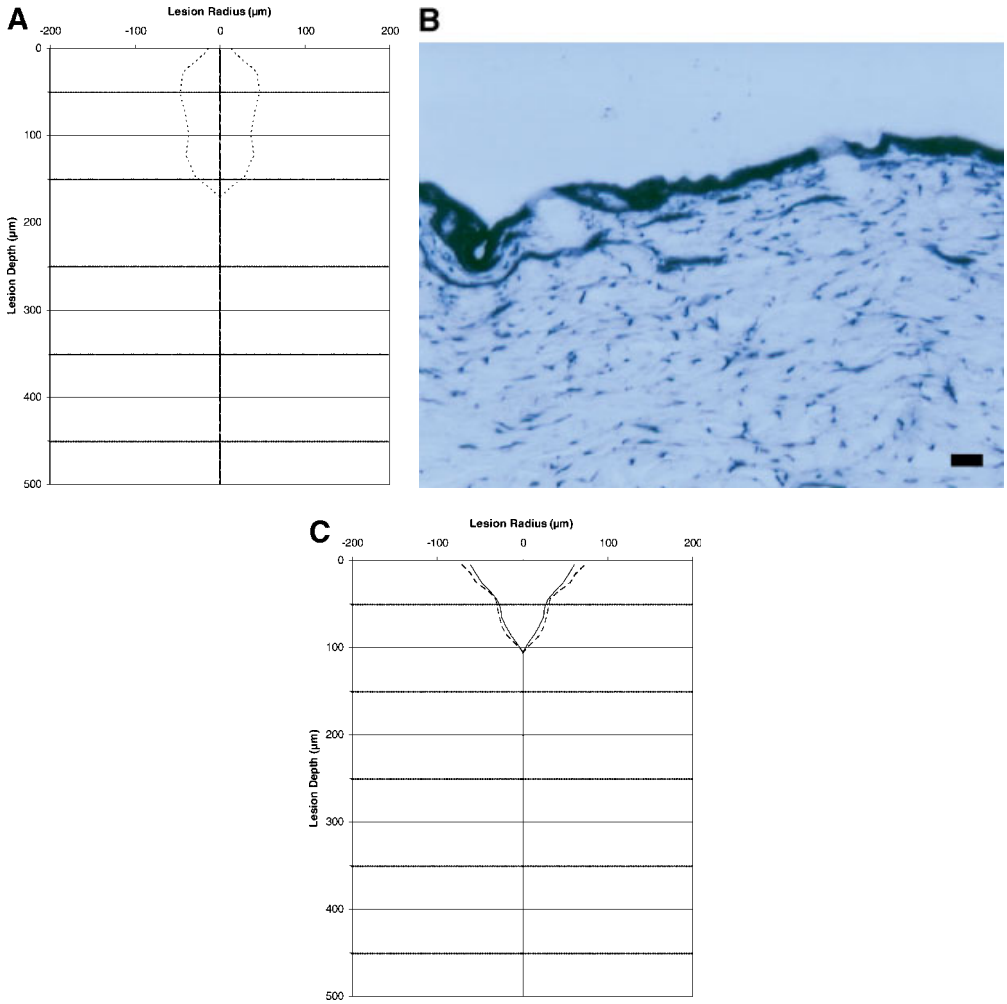

Fig. 3. Exposure parameters: 12 and 3 mJ, respectively, at a focal depth of 50 μm. **A**: Computer simulations of these treatment parameters. Contours are drawn for reaction coordinates of the Arrhenius model ($x = 10^{-2}$, 10^{0}, 10^{2}, and 10^{4}). Note: Only $x = 10^{4}$ is visible for (A) because the other contours have a radius of approximately 0 for all depths. **B**: NBTC-stained histologic sections of ex vivo facial skin, immediately after exposure (6×, scale bar, 50 μm). **C**: Statistical contours representing the extent of thermal damage. Note that depth of thermal damage is reduced substantially with reduced pulse energy. (Contours are drawn at diameters for which 80% and 90% of the lesions measured had diameters less than or equal to the contour diameter at that particular depth.) [Figure can be viewed in color online via www.interscience.wiley.com.]

tissue was $K_{th} = 0.005$ W/cm/K, and the specific heat (C) was taken to be $C = 3.7$ J/cm^3/K [21]. Thermal denaturation was assumed to follow an Arrhenius rate equation for the population of un-denatured protein.

$$-(1/n)\ (\mathrm{d}n/\mathrm{d}t) = R \equiv R_0 \exp(-T_1/T + T_1/T_0),$$

where T is the absolute temperature, $273 + T_{\mathrm{celsius}}$ and n is the mass density of the undenatured collagen. R is the rate of the forward reaction or the relative rate of decrease of n (i.e., $\mathrm{d}n/\mathrm{d}t = -nR$). The Arrhenius constants were selected so that $R = 10^3$/second at 65°C, and about 10^{-7}/second at 37°C. Thus, $T_0 = 338$ K, $R_0 = 10^3$/second, and $T_1 = 37{,}000$ K. Collagen denaturation is endothermic [25] with enthalpy $H = 45$ J/g. The tissue-heating rate is given by

$$\mathrm{d}/\mathrm{d}t(T + (1 - n/n_0)\Delta T) = W/C$$

where $\Delta T = C/H$, and W is the heating rate from the laser, and n_0 is the initial mass density of the undenatured collagen. Finally the reaction coordinate is

$$x = \int_{-\infty}^{t} R(t')\mathrm{d}t'.$$

The population fraction of the undenatured protein is e^{-x}.

Heat diffusion and thermal denaturation were treated in a split-step manner. The optical properties, including absorption and scattering, were assumed to be independent of the temperature and reaction coordinate. This removed the need for a time dependent model and meant that only one Monte Carlo calculation was needed. The output of these calculations is a contour plot showing the loci of constant reaction coordinate, x. Note that the volume

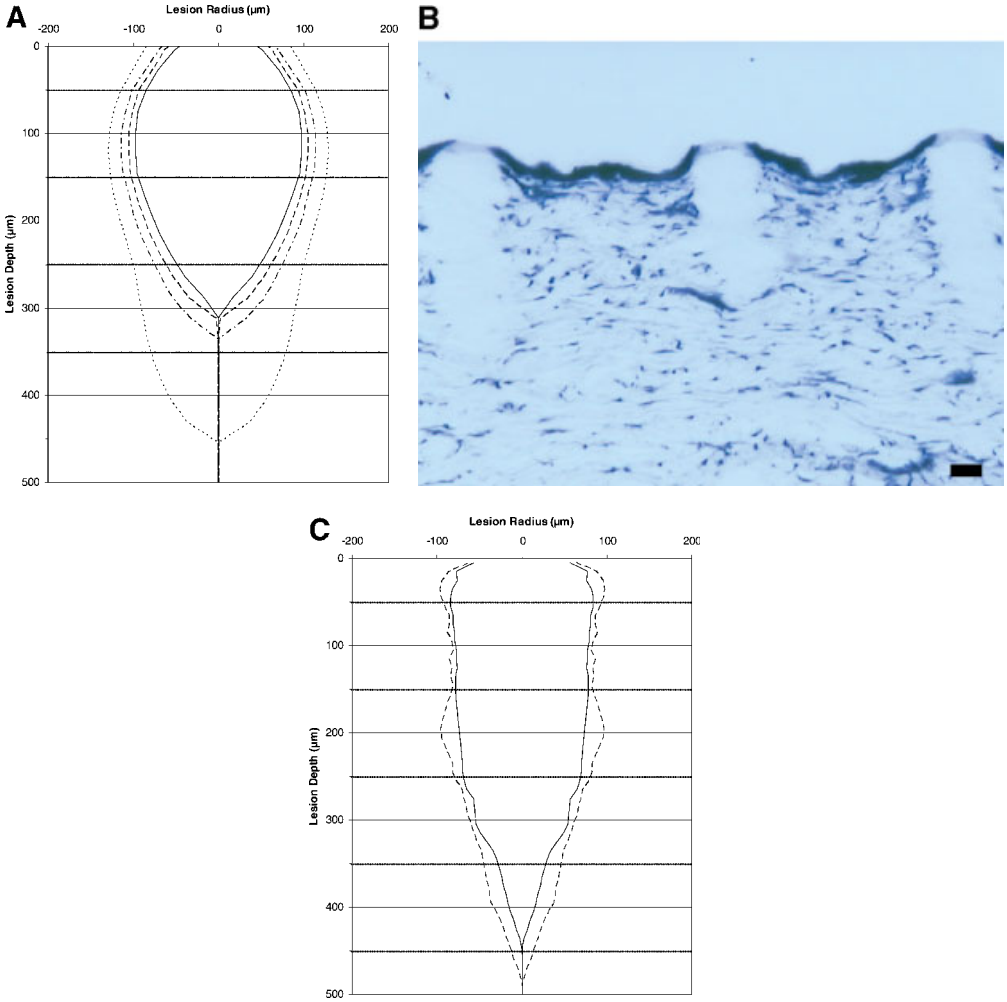

Fig. 4. Exposure parameters: 12 and 4 mJ, respectively, at a focal depth of 200 μm. **A**: Computer simulations of these parameters. **B**: NBTC-stained histologic sections of ex vivo facial skin, immediately after exposure (6×, scale bar, 50 μm). **C**: Statistical contours. Note that epidermal damage can be avoided by reducing the pulse energy. (Contours are drawn at diameters for which 80% and 90% of the lesions measured had diameters less than or equal to the contour diameter at that particular depth.) [Figure can be viewed in color online via www.interscience.wiley.com.]

enclosed in the contour $x = x_0$ varies weakly with x_0; its linear dimension increases by less than 50% when x_0 decreases by two orders of magnitude. This is attributed to the strong variation of the reaction rate with temperature. Note also that the value of x_0 is not independent of the choice of R_0. So no particular significance is attached to the value of x that best fits the data.

A large number of lesions created under various conditions were modeled. In general, the quoted tissue parameters gave quite a realistic picture of the shape and location of the lesions observed. Specific results of the ab initio calculations are shown in Figures 2–7, where contours for $x = 0.01$, 1, 100, and 10,000 are shown. In general, a reasonable fit to the shape of the lesions was consistently obtained using contours for $x \sim 100$, but the modeling typically placed the lesions slightly deeper in the tissue than the experiments showed. This difference is most likely the result of underestimating the width of the angular scattering distribution, but it could also be a result of underestimating the strength of the optical absorption, or of neglecting changes in tissue optical properties during irradiation. Minor alterations of the dimensions may also be explained by compression of the samples during the exposures.

RESULTS

Gross Appearance

Grossly, there was no apparent effect from any of the laser exposures. However, on 10× magnified examination, a precise array of small whitish dots could be seen which corresponded to the presence of photothermal lesions seen microscopically. With deeper focus and higher pulse energy exposures, dermatoglyph skin lines were distorted in a

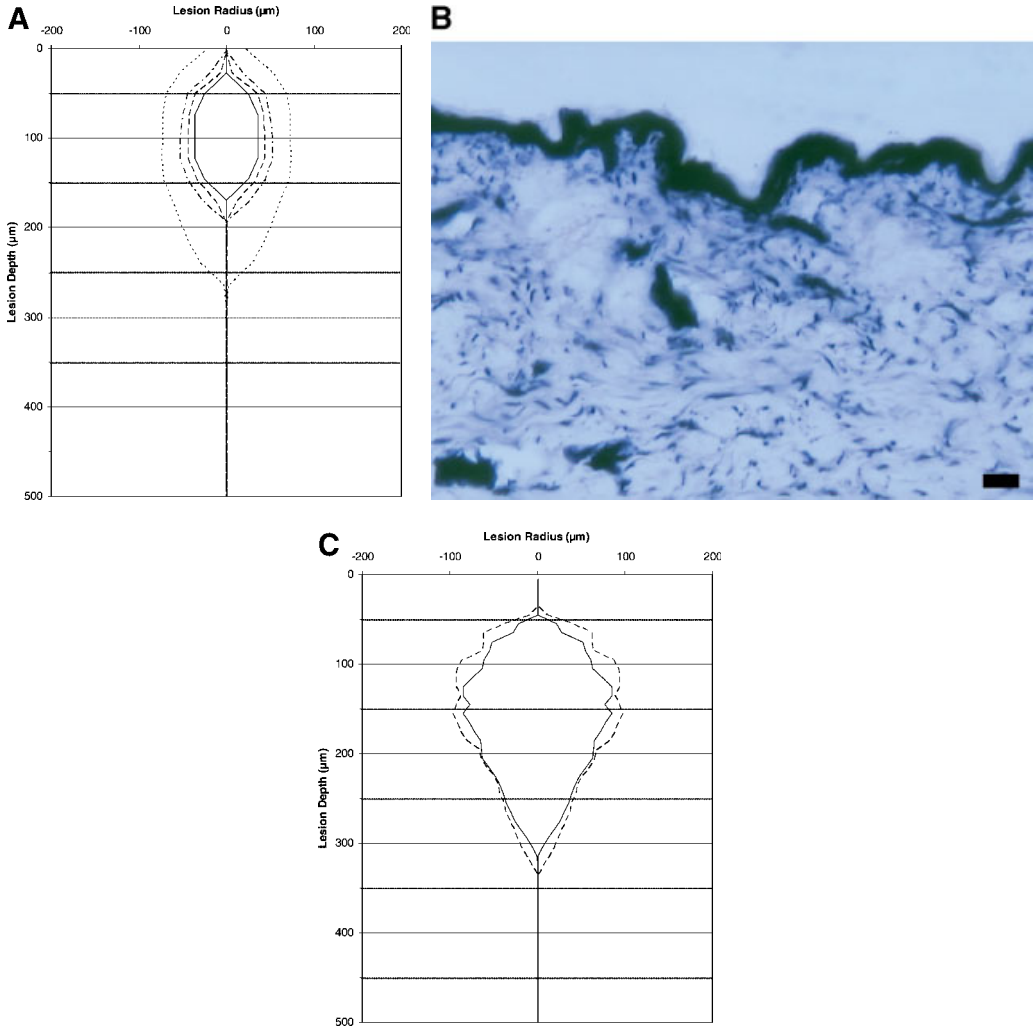

Fig. 5. Exposure parameters: 12 and 4 mJ, respectively, at a focal depth of 200 μm. **A**: Computer simulations of these parameters. **B**: NBTC-stained histologic sections of ex vivo facial skin, immediately after exposure (6×, scale bar, 50 μm). **C**: Statistical contours. Note that epidermal damage can be avoided by reducing the pulse energy. (Contours are drawn at diameters for which 80% and 90% of the lesions measured had diameters less than or equal to the contour diameter at that particular depth.) [Figure can be viewed in color online via www.interscience.wiley.com.]

radial pattern around each of the small dots, consistent with very local skin shrinkage at each lesion.

Focusing at 50-μm Depth

With the laser beam focused to a depth of 50 μm within the skin and pulse energy of 12 mJ (pulse duration of 12 milliseconds), the thermal damage lesions almost always involved the epidermis, with partial extension into the dermis (Fig. 2). Maximum depth of the damage from 12-mJ pulses was approximately 300 μm, and the maximum lesion diameter was about 200 μm, at the 90% contour. When pulse energy was reduced to 3 mJ (pulse duration of 3 milliseconds), the maximum depth of thermal damage was 100 μm and the maximum diameter was 100 μm for the 90% contour (Fig. 3). Shape of the damage pattern also changed, confining injury mainly to the epidermis.

Focusing at 200-μm Depth

With the laser beam focused 200 μm into the skin (i.e., within the papillary dermis) and pulse energy of 12 mJ (pulse duration 12 milliseconds), the maximum depth of damage was approximately 500 μm, with a 200 μm maximum diameter for the 90% contour (Fig. 4). Compared with the same pulse energy focused at 50-μm depth, these lesions clearly extended deeper into the dermis, yet had about the same width.

With a smaller pulse energy of 4 mJ focused at 200-μm depth (pulse duration 4 milliseconds, group 2 exposure of Table 1), the maximum depth of damage was limited to approximately 300 μm, and the uppermost 50 μm of tissue was spared (Fig. 5). Maximum lesion diameter again remained unchanged at a value of about 200 μm for the

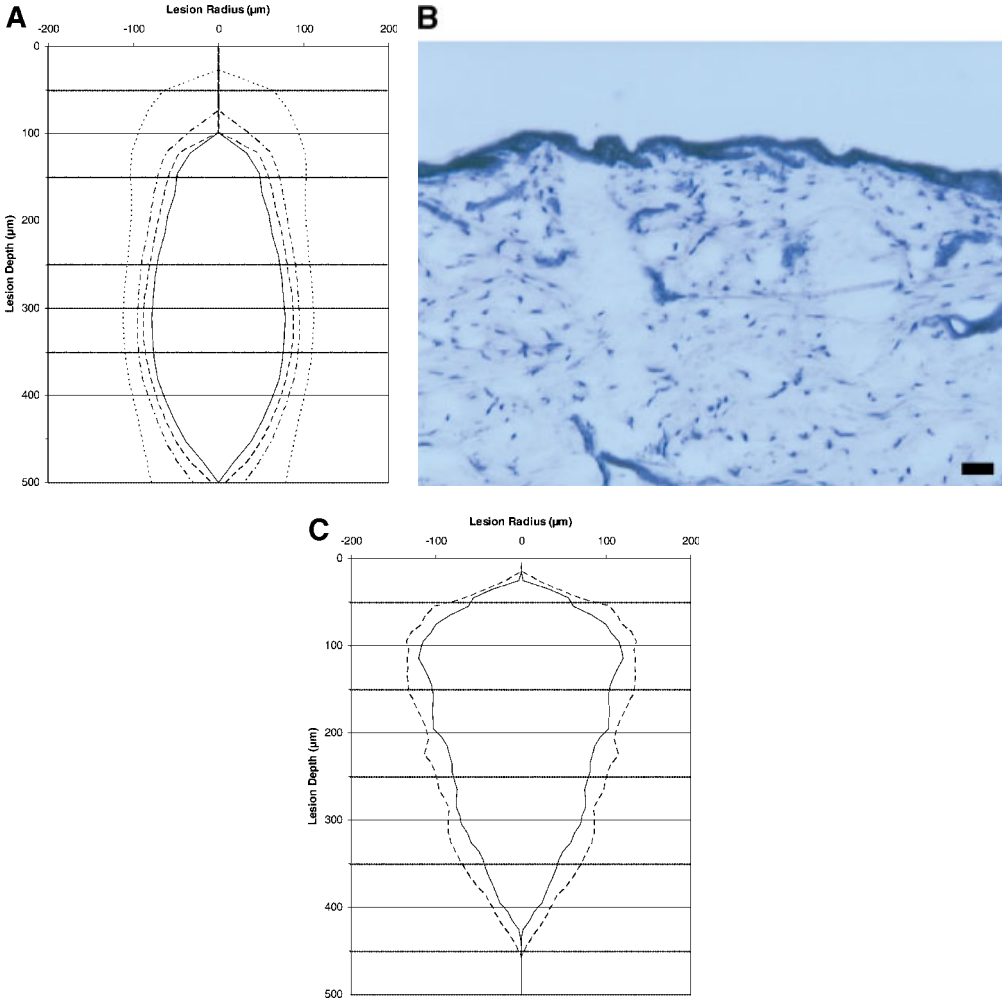

Fig. 6. Exposure parameters: 12 mJ at a focal depth of 450 μm. **A**: Computer simulation of the exposure parameters. **B**: NBTC stained histologic section of ex vivo facial skin, immediately after exposure (6×, scale bar, 50 μm). **C**: Statistical contours. Note that well-defined foci of thermal damage can be created in the papillary and upper reticular dermis with 12 mJ. (Contours are drawn at diameters for which 80% and 90% of the lesions measured had diameters less than or equal to the contour diameter at that particular depth.) [Figure can be viewed in color online via www.interscience.wiley.com.]

90% contour. Compared with 12-mJ pulse energy, the shape of lesions caused by 4-mJ pulses changed toward a spherical region of dermal damage, with sparing of the overlying epidermis.

Focusing at 450 μm Depth

With the laser beam focused at a depth of 450 μm in the skin and pulse energy of 12 mJ (pulse duration 12 milliseconds), a deeper elliptical lesion pattern with partial sparing of the epidermis was produced (Fig. 6). The maximum depth of thermal damage was 450 μm and the top 25–30 μm of the epidermis was spared for the 90% contour. The widest diameter was approximately 300 μm.

Focusing at 600 μm Depth

With the laser focused at a depth of 600 μm and pulse energy of 12 mJ (pulse duration 12 milliseconds), there was no observed change in the tissue. No lesions were detected in any skin sample exposed to these parameters. However, when pulse energy was increased to 20 mJ (pulse duration 20 milliseconds), well-defined intradermal lesions were created (Fig. 7). The maximum depth of damage was approximately 550 μm with a maximum width of approximately 250 μm for the 90% contour. The upper 25–30 μm of epidermis was spared for the 90% contour Additionally, dermal collagen denaturation can be seen clearly (Fig. 7D) by loss of collagen birefringence when viewed under cross-polarized light microscopy.

DISCUSSION

This ex vivo study shows that arrays of very small photothermal lesions can be created within human skin using a low power infrared laser device focused at high NA, at a wavelength absorbed primarily by tissue water. Epi-

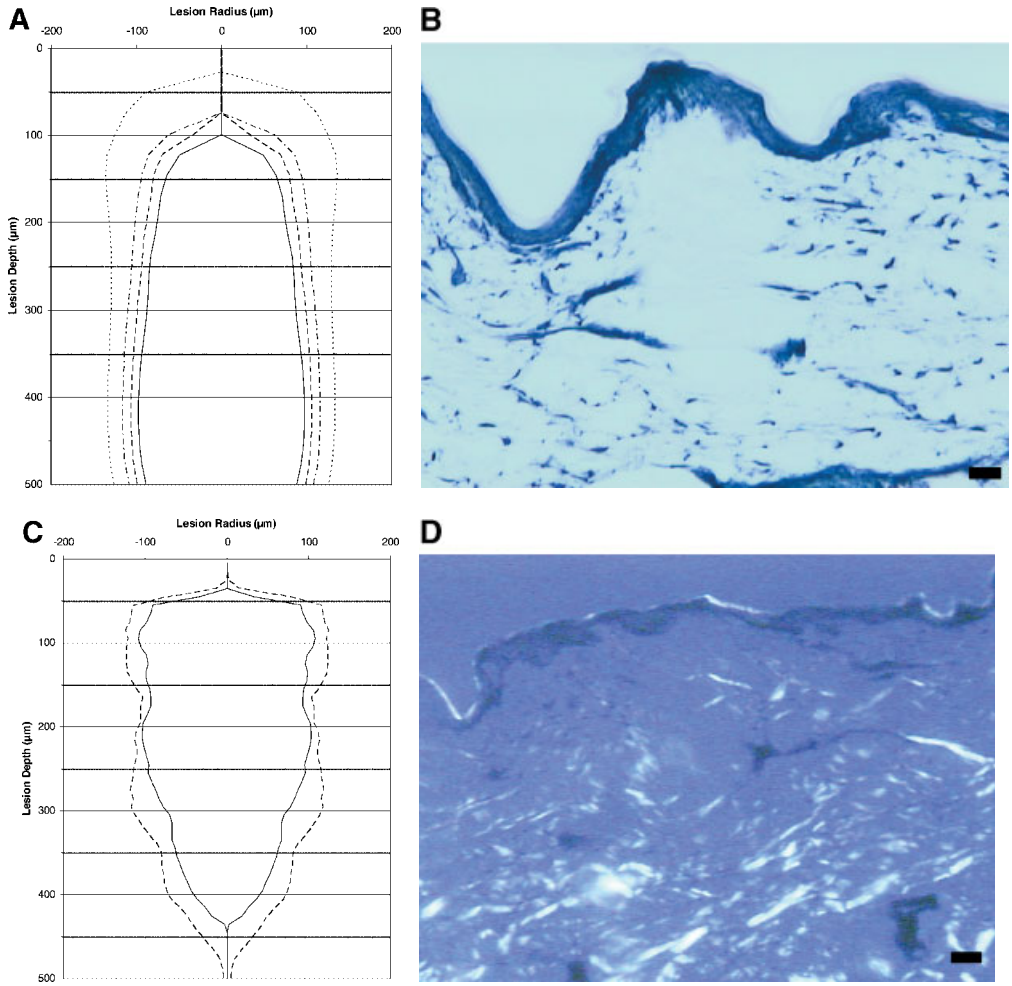

Fig. 7. Exposure parameters: 20 mJ, at a focal depth of 600 μm. **A**: Computer simulation model of these parameters. **B**: NBTC stained histologic section of ex vivo facial skin after exposure (6×, scale bar, 50 μm). **C**: Statistical contours of the thermal damage. (Contours are drawn at diameters for which 80% and 90% of the lesions measured had diameters less than or equal to the contour diameter at that particular depth.) **D**: Cross-polarized microscopy of the same section, showing loss of collagen birefringence in the focal areas of thermal damage. [Figure can be viewed in color online via www.interscience.wiley.com.]

dermis, papillary dermis, and/or reticular dermis can be arbitrarily chosen as primary sites for the photothermal lesions by adjusting focal depth and pulse energy. Localized thermal effects on cells and extracellular matrix were created, as evidenced by loss of LDH activity and collagen birefringence, respectively. Although laser microbeams have been used in experimental biology for decades [26], there are no therapeutic devices in dermatology using this conceptual approach. Recent advances with small semiconductor infrared lasers, miniature optics, and computer-driven beam controllers may soon allow this to change. It should be practical to create thousands or millions of microscopic foci of photothermal injury with controlled size, depth, and spacing, as a therapeutic stimulus in skin.

The size and location of cutaneous photothermal foci depend on a combination of optical parameters (e.g., wavelength, focusing optics, energy, pulse duration, tissue optical properties), and thermal parameters (e.g., skin temperature profile, skin cooling). As it penetrates skin, a focused laser beam is degraded by scattering, which in the infrared is mainly forward-directed, creating a blurred focal region. Therefore, the smallest focal spot that can be achieved necessarily enlarges with depth within the tissue. This is also the case when focused infrared beams are used for diagnostic imaging in skin, for example, for confocal laser scanning microscopy or optical coherence tomography. The quality of an optical focus within skin is difficult to model precisely; however, the maximum depth for which a useful "focal spot" can be achieved in unaltered skin, is probably about 1 mm. If optical scattering were decreased, for example, by pressurizing the skin or by injection of an optical clarifying agent such as glycerol [27], this depth

might be substantially increased. In this study, we have not investigated the effects of these factors. However, photothermal lesion width as measured by loss of LDH activity was maintained at about 200 μm even when the lesion extended deeply into the dermis. This width is about the same as the thermal damage zone produced around hair follicles or adult port wine stain vessels by SP with lasers or flashlamps.

Theoretically, the minimum photothermal damage size is on the same order of magnitude as a diffraction-limited focal spot within the tissue (i.e., several μm for the infrared optical region of the spectrum). As with SP, the concept of a "thermal relaxation time" for confinement of thermal injury is useful. To a first approximation, the region of high power density near the optical focus can be viewed as a cylinder oriented along the optical axis, with a minimum diameter equal to the focal spot size. In general, thermal relaxation time is given by $\tau \cong d^2/g\kappa$, where τ is thermal relaxation time, d is diameter, g is a geometric constant, and κ is the thermal diffusivity of the medium [14]. Thermal relaxation time in tissue for the nominally 20-μm diameter focal spot we used in this study, is about 0.5 milliseconds. With a laser power of only 1 W, we used exposure times from 3–20 milliseconds to achieve focal lesions about 200 μm in diameter, even at depths over 500-μm deep. Thermal conduction occurring during these pulses accounts in part for the photothermal lesions being much larger than the ~20-μm optical focus diameter. This was most apparent when the focus was placed only 50-μm deep, which would not be expected to cause significant broadening of the focal spot due to optical scattering. The smallest lesion width of about 100 μm in this study was achieved with the shortest pulse duration of 3 milliseconds (3-mJ pulse energy) and superficial focusing (50-μm focus depth). Extension of thermal damage due to exposures somewhat longer than the thermal relaxation time has been previously described in detail [28].

Focusing infrared lasers into skin as a means of therapy is not new. Muccini et al. reported local thermal damage to dermis followed by dermal remodeling, after focusing a 980-nm diode laser into dermis with a spherical focusing handpiece [29]. At 980 nm, however, hemoglobin and melanin are the dominant absorbing molecules in skin. Dermal injury at this wavelength therefore varies considerably with pigmentation and vascularity. This is not the case for infrared wavelengths longer than about 1,200 nm, for which water or lipids are the primary dermal chromophores. Manstein et al. reported foci of selective dermal damage with sparing of the epidermis with a focused infrared fiber laser operating at 1.06 and 1.2 μm, in combination with surface cooling and pulse durations of approximately 1 second. Such long exposure times limit the ability of these parameters to be used in commercial devices for the treatment of large areas [17].

This work was initiated with the intent of potentially providing a better-tolerated alternative to laser resurfacing for conditions such as scars, acne, and photoaged skin. Ablative methods using CO_2 and Er:YAG lasers have proven to be effective for the improvement of the skin surface and for the treatment of the above mentioned unwanted skin conditions. The major disadvantages of these ablative methods are pronounced side effects like oozing and erythema due to the complete removal of the epidermis. Nonablative collagen remodeling techniques have emerged in order to avoid these side effects. There is some evidence that the basic underlying mechanism of action is the induction of new collagen growth due to thermal damage of the dermis. It may not be necessary to cause gross damage of the epidermis in order to improve the surface. This study has shown that basically any three dimensional pattern of thermal damage can be achieved within a reasonable time. The thermal damage pattern may or may not include epidermal damage. The amount of epidermal damage can be varied by choice of the exposure parameters.

Clinical response to treatments with an array of microscopic thermal lesions remains unknown. Also, nothing is known about how to use this new approach in practice, for example, optimal lesion size, spacing, depth, shape, or degree of photothermal damage. It is also unknown whether epidermal injury should be included or excluded. However, the similarity of these thermal lesions to those created by SP strongly suggests that these thermal lesions will be very well tolerated when each individual lesion is fully surrounded by viable skin tissue that can initiate a rapid repair response. Moreover, the ability shown in this study to arbitrarily adjust size, depth, and density of photothermal lesions suggests that clinical responses can also be adjusted for a particular target, such as blood vessels and sebaceous glands. Since the dermal zones treated by this technique are completely denatured by the high local fluences that are used, it may be possible to kill blood vessels or sebaceous glands without damaging the epidermis. Further work needs to be done to investigate this. In essence, an array of lesions is equivalent to a precisely adjustable three-dimensional thermal burn. On one extreme, it is certain that a single microscopic thermal lesion will have essentially no therapeutic effect due to the small size of the lesion. On the other extreme, tightly packed lesions would create a two-dimensional burn, equivalent in many ways to laser resurfacing. Between these extremes, there may be a therapeutic range that avoids many of the side effects observed with full laser resurfacing, but achieves many of the same endpoints as resurfacing.

A similar comparison can be made for nonablative treatments. If the epidermis is spared, as proposed in this work, the resulting treatment would be similar to other nonablative treatment modalities, but without the need for cooling. It has been shown that nonablative treatments can be effective when sufficient pulse energies are used. However, it has also been shown that when pulse energies and numbers are increased to the point where a significant fraction of the treatment area is coagulated beneath the surface, scarring can result [30]. The proposed treatment methodology introduces a way to reproducibly control the fractional area of the tissue that is coagulated and thus may allow physicians to more reproducibly achieve therapeutic results with a lower risk of scarring.

Size, depth, maximum temperature, pattern, and density of small thermal lesions can potentially be used to control response, and should be clinically studied. The results of this in vitro study are instructive for how to choose exposure parameters for a specific thermal damage pattern. The optimum thermal damage pattern, however, remains subject to further investigation.

REFERENCES

1. Jaffe BH, Walsh JT, Jr. Water flux from partial-thickness skin wounds: Comparative study of the effects of Er:YAG and Ho:YAG lasers. Lasers Surg Med 1996;18(1):1–9.
2. Fitzpatrick RE. Maximizing benefits and minimizing risk with CO2 laser resurfacing. Dermatol Clin 2002;20(1):77–86.
3. Goldman MP, Roberts TL 3rd, Skover G, Lettieri JT, Fitzpatrick RE. Optimizing wound healing in the face after laser abrasion. J Am Acad Dermatol 2002;46(3):399–407.
4. Stuzin JM, Baker TJ, Baker TM, Kligman AM. Histologic effects of the high-energy pulsed CO2 laser on photoaged facial skin. Plast Reconstr Surg 1997;99(7):2036–2050.
5. Ross EV, McKinlay JR, Sajben FP, Miller CH, Barnette DJ, Meehan KJ, Chhieng NP, Deavers MJ, Zelickson BD. Use of a novel erbium laser in a Yucatan minipig: A study of residual thermal damage, ablation, and wound healing as a function of pulse duration. Lasers Surg Med 2002;30(2):93–100.
6. Seckel BR, Younai S, Wang KK. Skin tightening effects of the ultrapulse CO2 laser. Plast Reconstr Surg 1998;102(3):872–877.
7. Kligman AM, Zheng P, Lavker RM. The anatomy and pathogenesis of wrinkles. Br J Dermatol 1985;113(1):37–42.
8. Fisher GJ, Kang S, Varani J, Bata-Csorgo Z, Wan Y, Datta S, Voorhees JJ. Mechanisms of photoaging and chronological skin aging. Arch Dermatol 2002;138(11):1462–1670.
9. El-Domyati M, Attia S, Saleh F, Brown D, Birk DE, Gasparro F, Ahmad H, Uitto J. Intrinsic aging vs. photoaging: A comparative histopathological, immunohistochemical, and ultrastructural study of skin. Exp Dermatol 2002;11(5):398–405.
10. Kelly KM, Nelson JS, Lask GP, Geronemus RG, Bernstein LJ. Cryogen spray cooling in combination with nonablative laser treatment of facial rhytides. Arch Dermatol 1999;135(6):691–694.
11. Paithanker DY, Ross EV, Saleh BA, Blair MA, Graham BS. Acne treatment with a 1450 nm wavelength laser and cryogen spray cooling. Laser Surg Med 2002;31(2):106–114.
12. Trelles MA, Allones I, Luna R. Facial rejuvenation with a nonablative 1320 nm Nd:YAG laser: A preliminary clinical and histologic evaluation. Dermatol Surg 2001;27(2):111–116.
13. Maneker GM, Wrone DA, William RM, Moy RL. Treatment of facial rhytides with a non-ablative laser; a clinical and histologic study. Dermatol Surg 1999;25:440–444.
14. Anderson RR, Parrish JA. Selective photothermolysis: Precise microsurgery by selective absorption of pulsed radiation. Science 1983;220(4596):524–527.
15. Zelickson BD, Kilmer SL, Bernstein E, Chotzen VA, Dock J, Mehregan D, Coles C. Pulsed dye laser therapy for sun damaged skin. Laser Surg Med 1999;25(3):229–236.
16. Rajadhyaksha M, Grossman M, Esterowitz D, Webb RH, Anderson RR. In vivo confocal scanning laser microscopy of human skin: Melanin provides strong contrast. J Invest Dermatol 1995;104(6):946–952.
17. Manstein D, Poureshagh M, Yaroslavsky I, Altshuler GB, Anderson RR. Spatially confined photothermolysis of dermal targets using an IR-fiberlaser in combination with focusing and contact cooling. Lasers Surg Med 2002;14(Suppl):28.
18. Sumriddetchkajorn S, Riza NA. Micro-electro-mechanical system-based digitally controlled optical beam profiler. Appl Opt 2002;41(18):3506–3510.
19. Smith KJ, Skelton HG, Graham JS, Hamilton TA, Hackley BE, Jr., Hurst CG. Depth of morphologic skin damage and viability after one, two, and three passes of a high-energy, short-pulse CO2 laser (Tru-Pulse) in pig skin. J Am Acad Dermatol 1997;37(2 pt 1):204–210.
20. Chung JH, Koh WS, Youn JI. Histological responses of port wine stains in brown skin after 578 nm copper vapor laser treatment. Lasers Surg Med 1996;18(4):358–366.
21. Ashley J. Welch, Martin J.C. Van Gemert, editors. Optical thermal response of laser-irradiated tissue. NY: Plenum Press; 1995.
22. Henyey LG, Greenstein JL. Diffuse radiation in the galaxy. Astrophys J 1941;93:70–83.
23. Palmer KF, Williams D. Optical properties of water in the near infrared. J Opt Soc Am 1974;64:1107–1110.
24. Press WH, Vettering WT, Teukolsky SA, Flannery BP. Chapter 19. Numerical Recipes in Fortran 77. Cambridge, UK, NY and Australia: Cambridge University Press; 1992.
25. McClain PE, Wiley ER. Differential scanning calorimeter studies of the thermal transitions of collagen. J Biol Chem 1972;247:692–697.
26. Konig K, Liang H, Berns MW, Tromberg BJ. Cell damage by near-IR microbeams. Nature 1995;377(6544):20–21.
27. Vargas G, Readinger A, Dozier SS, Welch AJ. Morphological changes in blood vessels produced by hyperosmotic agents and measured by optical coherence tomography. Photochem Photobiol 2003;77(5):541–549.
28. Altshuler GB, Anderson RR, Manstein D, Zenzie HH, Smirnov MZ. Extended theory of selective photothermolysis. Laser Surg Med 2001;29(5):416–432.
29. Muccini JA, Jr., O'Donnell FE, Jr., Fuller T, Reinisch L. Laser treatment of solar elastosis with epithelial preservation. Lasers Surg Med 1998;23(3):121–127.
30. Ross EV, Sajben FP, Hsia J, Barnette D, Miller CH, McKinlay JR. Nonablative skin remodeling: Selective dermal heating with a mid-infrared laser and contact cooling combination. Lasers Surg Med 2000;26(2):186–195.